Pergamon

Int. J. Heat Mass Transfer. Vol. 38, No. 7, pp. 1237–1247, 1995

0017–9310/95 $9.50 + 0.00

0017–9310(94)00240–1

Latent heat method for solidification process of a binary alloy system

S. L. LEE

Department of Power Mechanical Engineering, National Tsing-Hua University, Hsinchu 30043, Taiwan

and

R. Y. TZONG

Vero Veria Corporation Co. Ltd, 105 Sec. 4, San-ho Road, Sanchung, Taipei 24153, Taiwan

(*Received* 10 *November* 1993 *and in final form* 22 *July* 1994)

Abstract—A latent heat method is modified in the present study to properly handle the latent heat evolved in the solidification process of a binary alloy system. The eutectic state (C_E, T_E) is imposed on the eutectic front such that no species equation is needed in the pure solid region. Both momentum and species equations in the irregular domain consisting of the mushy zone and the liquid region are successfully solved by using the weighting function scheme along with the NAPPLE algorithm. To trace the interface of the mushy zone and the pure liquid region, an interpolation technique is proposed. Two examples were conducted to examine the performance of the present method. Satisfactory agreement with the existing experimental results is observed on the total volume of the mushy zone.

INTRODUCTION

Solidification of an alloy has many industrial applications, such as foundry technology, crystal growth, coating and purification of materials, welding process, etc. Unlike the classical Stefan problem, however, alloy solidification involves complex heat and mass transport phenomena that are still not well understood. For most metal alloys, there could be three regions, namely, solid region, mushy zone (dendrite arms and interdendritic liquid) and liquid region in solidification process. To investigate the heat and mass transfer during the solidification process of an alloy, a few models have been proposed. They can be roughly classified into the continuum model and the volume-averaged model.

Based on principles of classical mixture theory, Bennon and Incropera [1–3] developed a continuum model for momentum, heat and species transport in the solidification process of a binary alloy. Voller *et al.* [4] and Rappaz and Voller [5] modified the continuum model by considering the solute distribution on microstructure (Scheil approach). Recently, Beckermann and Viskanta [6] reported an experimental study on dendritic solidification of an ammonium chloride–water solution (NH_4Cl–H_2O). A numerical simulation for the same physical configuration was also performed using a volumetric averaging technique. Subsequently, the volumetric averaging technique was systematically derived by Ganesan and Poirier [7] and Ni and Beckermann [8]. Detailed discussions on microstructure formation and mathematical modeling of transport phenomenon during solidification of binary systems can be found in the reviews [9, 10].

As pointed out by Flemings, some eutectic will form in the solidification process of an alloy, no matter how low the initial composition (see p. 143 of ref. [11]). Therefore, a great amount of latent heat could be suddenly released in an area where the eutectic front is sweeping through. This would lead to a numerical instability without a particular treatment on the evolution of latent heat. Another numerical difficulty could also arise from the species equation. It is easy to verify that the species equation will become trivial in the pure solid region due to a zero diffusion coefficient. This might result in an inaccurate estimation on the amount of rejected solute when the interdendritic liquid solidifies upon sweeping of a eutectic front. The previous investigators [4, 6] did not consider a binary system that was cooled below its eutectic point, and thus did not observe these phenomena.

In the present study, microstructure formation of the mushy zone and its relation to the phase diagram is elucidated. Understanding the role of phase diagram in solidification process of an alloy is essential to modeling the related transport phenomenon. The abrupt evolution of latent heat from the eutectic front is treated by employing the latent heat method [12]. Through the use of the weighting function scheme [12, 13], the eutectic concentration C_E is imposed on the eutectic front (the isotherm of $T = T_E$) such that the

NOMENCLATURE

C	solute concentration
C_p	specific heat [J kg^{-1} K^{-1}]
D	solute diffusivity [m^2 s^{-1}]
d	dendrite arm diameter [m]
Da	Darcy number, K/L^2
F	inertia coefficient, equation (19b)
f	liquid fraction inside a control volume, $G\varepsilon$
G	fraction of mushy zone plus liquid region inside a control volume
g	gravity, 9.81 m s^{-2}
H	enthalpy [J kg^{-1}]
K	permeability function [m^2], equation (19a)
k	thermal conductivity [W m^{-1} K^{-1}]
L	latent heat [J kg^{-1}] or characteristic length [m]
Le	Lewis number, α_ℓ/D_ℓ
N	ratio of solute buoyancy and thermal buoyancy, $\beta_C C_E/\beta_T \Delta T$
P, p	pressure and dimensionless pressure, $p = P/\rho_\ell V_c^2$
Pr	Prandtl number, ν/α_ℓ
Ra	Rayleigh number, $g\beta_T \Delta T L^3/\alpha_\ell \nu$
Ste	Stefan number, $(C_p)_\ell \Delta T/\Delta H$
T	temperature [K]
t	time [s]
t_c	characteristic time, $L^2/(\sigma\alpha_\ell)$
Tol	tolerance defined in equation (25)
U, V	velocity components in X- and Y-directions [m s^{-1}]
u, v	dimensionless velocity components, $u = U/V_c$ and $v = V/V_c$
$\mathbf{v}$	dimensionless velocity vector, $u\mathbf{i}+v\mathbf{j}$
V_c	characteristic velocity [m s^{-1}], α_ℓ/L
X, Y	coordinate system [m]
x, y	dimensionless coordinate system, $x = X/L$ and $y = Y/L$
x_E, x_T	locations of eutectic front and the line of dendrite tips in example 1.

Greek symbols

α	thermal diffusivity [m^2 s^{-1}]
β	density ratio, ρ_s/ρ_ℓ
β_C	concentration expansion coefficient
β_T	thermal expansion coefficients [K^{-1}]
γ	ratio of specific heat, $(\rho C_p)_s/(\rho C_p)_\ell$
Δ	difference quantity
ΔH	heat of fusion [J kg^{-1}]
ε	porosity
θ	dimensionless temperature, $(T-T_\infty)/\Delta T$
κ	equilibrium partition ratio, C_S/C_L
Λ	sensible heat [J kg^{-1}]
μ	dynamic viscosity [kg m^{-1} s^{-1}]
ν	kinematic viscosity [m^2 s^{-1}]
ρ	density [kg m^{-3}]
σ	dimensionless parameter, $Ste/(1+Ste)$
τ	dimensionless time, t/t_c
Φ, Φ^*	artificial functions, equation (24)
ϕ	normalized concentration in liquid phase, C_ℓ/C_E
ψ	stream function, equation (34).

Superscripts

$\bar{}$	averaged quantity inside a control volume
*	dimensionless quantity
$\tilde{}$	guessed quantity.

Subscript

0	initial quantity
∞	ambient condition
c	characteristic quantity
E	eutectic state
eff	effective
F	freezing point when $C = 0$
L	liquidus
ℓ	liquid phase
max	maximum
min	minimum
ref	reference
S	solidus
s	solid phase.

eutectic front is always at the state of eutectic point (C_E, T_E). Thus, no species equation is needed in the pure solid region. Two examples are illustrated to examine the performance of the present method.

THEORETICAL ANALYSIS

Consider a superheated binary alloy of concentration C_0 and temperature T_0 being cooled to a temperature T_∞ below its eutectic temperature T_E (i.e. $T_0 > T_L > T_E > T_\infty$, where T_L denotes the liquidus). The solidification process is assumed to be in thermal equilibrium. Figure 1 shows a cooling process of this type in a schematic phase diagram. As illustrated in Fig. 1, the first solid would begin to form at $T_L(C_0)$ with the concentration $\kappa\, C_0$ (see path a), where $\kappa = C_S(T)/C_L(T)$ is known as the equilibrium partition ratio. For most alloys, the equilibrium partition ratio κ is less than unity, such that the rejected solute $(1-\kappa)C_0$ enriches the concentration of the liquid phase to state A. This would give rise to an increase in the solute concentration of the subsequently solidified alloy as illustrated by path b. It appears that the liquid phase will eventually reach the eutectic point (C_E, T_E)

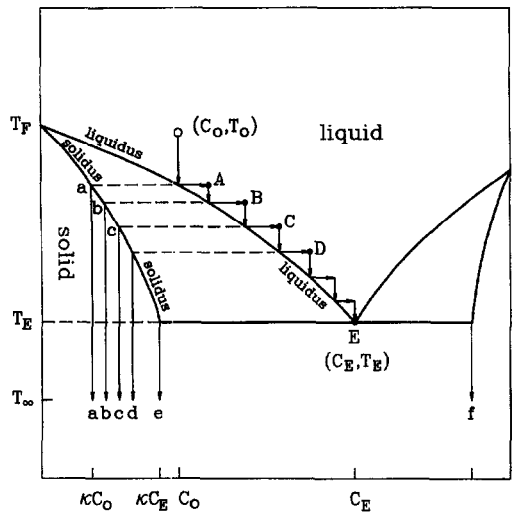

Fig. 1. Solidification process on a schematic phase diagram of a binary alloy system.

as long as $C_0 \neq 0$. After that the liquid phase solidifies like a pure substance.

For most metal alloys, the solute diffusivity D is far smaller than the thermal diffusivity α (i.e. $Le = \alpha/D \gg 1$). This will build up a layer of solute-rich liquid in front of the liquid–solid interface. The enriched solute decreases the liquidus and thus depresses the solidification process or even remelts the solid phase. Under such a situation, the liquid–solid interface would grow into a dendritic form [11, 14]. Figure 2 presents a typical dendritic solidification (i.e. the secondary dendrite arms are not shown here for simplicity). The region beyond the line of dendrite tips is the liquid region, while that beneath the dendrite root (eutectic front) is the solid region. The two-phase region including the dendrites and the interdendritic liquid is known as the mushy zone. As depicted in the mushy zone of Fig. 2, the solidified alloy following paths *a–d* (see Fig. 1) would form the dendrite trunk, while the surface of the dendrite trunk is at the liquidus (states A, B, C, D from the tip to the root of the dendrite). The liquid at the root of the dendrite trunk, however, is at the eutectic point E. It would form a eutectic alloy $(e+f)$ after solidification. Thus, the triangle area enclosed by the liquidus, the solidus and

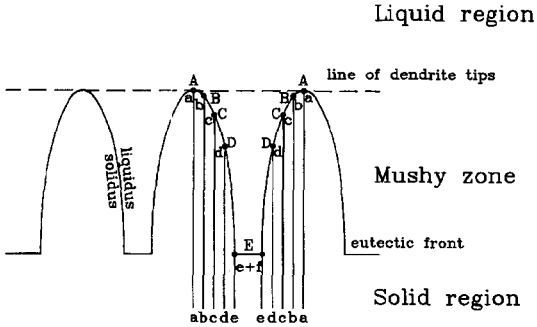

Fig. 2. Macro-microstructure of the mushy zone.

the eutectic line in a phase diagram (Fig. 1) does not exist physically.

Generally speaking, the spacing between two adjacent dendrite trunks (primary spacing) is only 10–100 μm as compared to the height of the dendrite trunk, which could be as large as 100 mm. As a result, the concentration gradient of the solute in the interdendritic liquid is essentially parallel to the dendrite trunk (see Fig. 2). In addition, a control volume of practical size for numerical procedure (say 5×5 mm) would cover hundreds of dendrite trunks. This implies a uniformly distributed solute concentration in the liquid phase of the control volume. On the other hand, inside the dendrite trunks, the solute concentration varies from $\kappa\, C_0$ (path *a*) in the center to $\kappa\, C_E$ on the root surface. Such a concentration variation is negligibly small as compared to the high concentration in the liquid phase, especially when the equilibrium partition ratio κ is small. Based on the physical reasoning, both dendrite and interdendritic liquid could be assumed to possess their own uniform solute concentration inside a control volume. Such an assumption (known as the level rule) is evidenced from many photomicrographs of dendritic structures such as those in Figs. 3–19 and 5–11 of ref. [11]. Thus, the average solute concentration inside a control volume is expressible as

$$\bar{\rho}\,\bar{C} = \varepsilon\,\rho_\ell\,\bar{C}_\ell + (1-\varepsilon)\,\rho_S\,\bar{C}_S = [\varepsilon\,\rho_\ell + (1-\varepsilon)\,\rho_S\,\kappa]\,C_\ell \quad (1)$$

where $\bar{\rho} = \varepsilon\,\rho_\ell + (1-\varepsilon)\,\rho_S$ is the average density and ε is the porosity (i.e. the fraction of liquid by volume) of the mushy zone. The notations $\bar{C}_\ell$ and $\bar{C}_S$ denote the average solute concentrations in the interdendritic liquid and inside the dendrite arms, respectively, while C_ℓ is the solute concentration of the liquid phase (i.e. $C_\ell \approx \bar{C}_\ell \approx C_L$). In the derivation of equation (1), both liquid phase and solid phase inside the control volume are assumed to possess the same temperature T (thermally equilibrium) such that

$$\bar{C}_S/\bar{C}_\ell \approx C_S(T)/C_L(T) = \kappa(T) \quad (2)$$

makes a good approximation.

Next, assume stationary solid phase and introduce the conservation law for the solute concentration on the control volume. This yields the species equation [6]:

$$\frac{\partial(\bar{\rho}\bar{C})}{\partial t} + \rho U\frac{\partial C_\ell}{\partial X} + \rho V\frac{\partial C_\ell}{\partial Y} = \frac{\partial}{\partial X}\left(\bar{\rho}\,\bar{D}_{\text{eff}}\frac{\partial C_\ell}{\partial X}\right) + \frac{\partial}{\partial Y}\left(\bar{\rho}\,\bar{D}_{\text{eff}}\frac{\partial C_\ell}{\partial Y}\right) \quad (3)$$

where $(U, V) = (\varepsilon U_\ell, \varepsilon V_\ell)$ is the superficial velocity, while (U_ℓ, V_ℓ) is the velocity of the interdendritic liquid. The effective diffusivity of the solute ($\bar{D}_{\text{eff}}$) and the unsteady term $\partial(\bar{\rho}\,\bar{C})/\partial t$ could be approximated, respectively, by

$$\bar{\rho}\bar{D}_{\text{eff}} = \varepsilon\rho_\ell D_{\ell,\text{eff}} + (1-\varepsilon)\rho_S D_{s,\text{eff}} \approx \varepsilon\rho_\ell D_{\ell,\text{eff}} \quad (4)$$

$$\frac{\partial(\bar{\rho}\bar{C})}{\partial t} = [\varepsilon + (1-\varepsilon)\beta\kappa]\rho_\ell \frac{\partial C_\ell}{\partial t} + (1-\beta\kappa)\rho_\ell C_\ell \frac{\partial \varepsilon}{\partial t} \quad (5)$$

with $\beta = \rho_S/\rho_\ell$ being the density ratio of the solid phase and liquid phase. It is interesting to note that the second term on the right-hand side of equation (5) is the source of the solute concentration. It comes from the rejected solute when a liquid particle solidifies.

Similarly, the energy equation can be written as

$$\frac{\partial(\bar{\rho}\bar{H})}{\partial t} + U\frac{\partial \Lambda_\ell}{\partial X} + V\frac{\partial \Lambda_\ell}{\partial Y} = \frac{\partial}{\partial X}\left(k_{\text{eff}}\frac{\partial T}{\partial X}\right) + \frac{\partial}{\partial Y}\left(k_{\text{eff}}\frac{\partial T}{\partial Y}\right) \quad (6)$$

$$\frac{\partial \Lambda_\ell}{\partial X} = \rho_\ell (C_p)_\ell \frac{\partial T}{\partial X} \quad (7)$$

where Λ_ℓ and $(C_p)_\ell$ are the sensible heat and specific heat of liquid phase, and $\bar{H}$ is the average enthalpy of liquid and solid phases inside the control volume. As in the numerical procedure of the latent heat method for pure substance [12], the enthalpy $\bar{H}$ is split up into latent heat and sensible heat as

$$\frac{\partial(\bar{\rho}\bar{H})}{\partial t} = \bar{\rho}\bar{C}_p\frac{\partial T}{\partial t} + \frac{\partial(\bar{\rho}L)}{\partial t} \quad (8)$$

$$\bar{\rho}\bar{C}_p = f\rho_\ell (C_p)_\ell + (1-f)\rho_S (C_p)_S \quad (9)$$

$$\bar{\rho}L = f\rho_\ell \Delta H \quad (10)$$

where $\bar{C}_p$ is the average specific heat of the liquid and solid phases and f denotes the fraction of liquid phase inside the control volume. It appears that the f-value would be equal to the porosity when the control volume is located in one of the three regions, namely, the liquid region, the mushy zone and the solid region. However, care must be exercised when a control volume covers both the solid region and mushy zone, where ε could have a sharp jump across the eutectic front. Suppose that a eutectic front intersects a control volume at an instant. Let $(1-G)$ be the fraction of solid region and ε be the porosity of the mushy zone ($\varepsilon = 1$ in liquid region), then the fraction of liquid inside the control volume can be written as

$$f = G\varepsilon. \quad (11)$$

Thanks to the fact that the eutectic front is at the state of (C_E, T_E), the G value can be easily evaluated by tracing the isotherm of $T = T_E$ with a technique proposed in ref. [12].

In equation (10), ΔH is the latent heat of fusion of the alloy, while L is the latent heat per unit mass inside the control volume. Strictly speaking, the heat of fusion (ΔH) depends on the solute concentration. As a result, its value would vary from time to time and from one location to another due to solute rejection and diffusion during the solidification process. In the present investigation, however, the heat of fusion will be regarded as a constant to simplify the computations. The heat of fusion based on the initial solute concentration in the liquid phase (C_0 for example) would make good approximation for the value of this constant. Similar treatment has been widely employed in the past [6, 15]. Note that in the formulation of the continuum model [1–5] enthalpy for each phase (solid and liquid) should be defined such that the energy equation governs the 'mixture enthalpy' of the system. Unfortunately, the enthalpy defined by Bennon and Incropera [1–3] and Voller *et al.* [4] and Rappaz and Voller [5] leads to a heat of fusion $\Delta H(T) = [(C_p)_S - (C_p)_\ell]\ (T - T_E) + (\Delta H)_E$ that depends on the specific heat of both solid and liquid phases. This seems physically impossible.

Due to the lack of a reliable model, the superficial velocity (U, V) needed in solving equations (3) and (6) for the mushy zone is determined by the use of the well-known model for non-Darcy porous media [6]. After introducing the dimensionless transformation

$$x = X/L \quad y = Y/L \quad \tau = t/t_c \quad u = U/V_c \quad v = V/V_c$$

$$p = P/\rho_\ell V_c^2 \quad \theta = (T - T_\infty)/\Delta T \quad \Delta T = T_0 - T_\infty$$

$$\phi = C_\ell/C_E, \quad \nu_{\text{eff}}^* = \nu_{\text{eff}}/\nu \quad k_{\text{eff}}^* = k_{\text{eff}}/k_\ell$$

$$D_{\text{eff}}^* = D_{\text{eff}}/D_\ell \quad \gamma = (\rho C_p)_s/(\rho C_p)_\ell \quad V_c = \alpha_\ell/L$$

$$t_c = L^2/(\sigma\alpha_\ell)$$

$$\sigma = Ste/(1 + Ste) \quad (12)$$

along with the physical parameters

$$Pr = \nu/\alpha_\ell \quad Ste = (C_p)_\ell \Delta T/\Delta H \quad Da = K/L^2$$

$$Ra = g\beta_T \Delta T L^3/\alpha_\ell \nu \quad N = \beta_C C_E/\beta_T \Delta T$$

$$Le = \alpha_\ell/D_\ell \quad (13)$$

the governing equations are expressible as

$$\sigma(1-\beta)\frac{\partial \varepsilon}{\partial \tau} + \frac{\partial u}{\partial x} + \frac{\partial v}{\partial y} = 0 \quad (14)$$

$$\frac{\sigma}{\varepsilon}\frac{\partial u}{\partial \tau} + \frac{u}{\varepsilon^2}\frac{\partial u}{\partial x} + \frac{v}{\varepsilon^2}\frac{\partial u}{\partial y} = -\frac{\partial p}{\partial x} + \frac{Pr}{\varepsilon}\nu_{\text{eff}}^*\left[\frac{\partial^2 u}{\partial x^2} + \frac{\partial^2 u}{\partial y^2}\right] - \left(\frac{Pr}{Da} + \frac{F}{\sqrt{Da}}|\mathbf{v}|\right)u \quad (15)$$

$$\frac{\sigma}{\varepsilon}\frac{\partial v}{\partial \tau} + \frac{u}{\varepsilon^2}\frac{\partial v}{\partial x} + \frac{v}{\varepsilon^2}\frac{\partial v}{\partial y} = -\frac{\partial p}{\partial y} + \frac{Pr}{\varepsilon}\nu_{\text{eff}}^*\left[\frac{\partial^2 v}{\partial x^2} + \frac{\partial^2 v}{\partial y^2}\right] - \left(\frac{Pr}{Da} + \frac{F}{\sqrt{Da}}|\mathbf{v}|\right)v + Ra\,Pr\,[(\theta - \theta_{\text{ref}}) + N(\phi - \phi_{\text{ref}})] \quad (16)$$

$$\sigma\bar{\gamma}\frac{\partial\theta}{\partial\tau}+(1-\sigma)\frac{\partial f}{\partial\tau}-u\frac{\partial\theta}{\partial x}+v\frac{\partial\theta}{\partial y}=\frac{\partial}{\partial x}\left(k^*_{\text{eff}}\frac{\partial\theta}{\partial x}\right)+\frac{\partial}{\partial y}\left(k^*_{\text{eff}}\frac{\partial\theta}{\partial y}\right) \quad (17)$$

$$\sigma[\varepsilon+(1-\varepsilon)\beta\kappa]\frac{\partial\phi}{\partial\tau}+(1-\beta\kappa)\phi\frac{\partial\varepsilon}{\partial\tau}+u\frac{\partial\phi}{\partial x}+v\frac{\partial\phi}{\partial y}=\frac{\partial}{\partial x}\left(\varepsilon Le^{-1}D^*_{\text{eff}}\frac{\partial\phi}{\partial x}\right)+\frac{\partial}{\partial y}\left(\varepsilon Le^{-1}D^*_{\text{eff}}\frac{\partial\phi}{\partial y}\right) \quad (18)$$

where $|\mathbf{v}|=(u^2+v^2)^{1/2}$ denotes the magnitude of the velocity, while the permeability function K, the inertia coefficient F and the dendrite arm diameter d are approximated by

$$K=\frac{d^2\varepsilon^3}{180(1-\varepsilon)^2} \quad (19a)$$

$$F=0.13\varepsilon^{-1.5} \quad (19b)$$

$$d\approx 100\ \mu\text{m}. \quad (19c)$$

Generally speaking, the shrinkage-caused flow is negligibly small as compared to the buoyancy-driven flow, such that the continuity equation (14) reduces to

$$\frac{\partial u}{\partial x}+\frac{\partial v}{\partial y}=0. \quad (20)$$

For simplicity, the average heat capacity $\bar{\gamma}$ and the effective thermal conductivity k^*_{eff} in equation (17) for each control volume are approximated by

$$\bar{\gamma}=f+(1-f)\gamma \quad (21)$$

$$k^*_{\text{eff}}=f+(1-f)k_s/k_\ell. \quad (22)$$

It is noted that the entire domain including the solid region, mushy zone and the liquid region can be treated as a single body when the energy equation (17) is solved for the temperature θ. Unfortunately, the species equation (18) becomes trivial in the solid region due to its zero diffusion coefficient. A similar situation occurs in the momentum equations when the pressure solution is attempted. To circumvent this difficulty, the particular characteristic ($\phi=1$) along with the no-slip condition ($u=v=0$) is imposed at the eutectic front such that there is no need to solve the solution (u,v,p,ϕ) for the solid region. This implies that the mushy zone and the liquid region should be regarded as a single body having an irregular shape when equations (15), (16), (18) and (20) are solved. The weighting function scheme [12] along with the NAPPLE algorithm [16] was found to solve the solution (u,v,p,ϕ) quite effectively on such an irregular shape of domain.

In the numerical procedure, the porosity ε for each control volume should be guessed before the system of governing equations is solved. After that, the porosity is updated from the level rule

$$\varepsilon=\frac{\bar{\rho}\bar{C}-\rho_S C_S(T)}{\rho_\ell C_L(T)-\rho_S C_S(T)}=\frac{(\bar{\rho}\bar{C}/\rho_\ell C_L)-\beta\kappa}{1-\beta\kappa}=\left(\frac{\beta\kappa}{1-\beta\kappa}+\tilde{\varepsilon}\right)(\phi/\phi_L)-\frac{\beta\kappa}{1-\beta\kappa} \quad (23)$$

where $\tilde{\varepsilon}$ is the porosity at previous iteration and T (or θ) is the temperature of the control volume. The symbol ϕ_L denotes the solute concentration at the liquidus corresponding to the temperature of the control volume, while the equilibrium partition ratio κ (being a function of T) is not necessarily a constant.

It should be noted here that the porosity ε is unity in the entire liquid region including the line of dendrite tips. This renders the line of dendrite tips (see Fig. 2) very difficult to trace. Conventionally, the line of dendrite tips is determined by tracing the curve of $\varepsilon=0.999$ [6]. Such a definition, however, would provide a zigzag curve for the line of dendrite tips. In the present investigation, an artificial function Φ^* is defined by

$$\Phi^*=\Phi \quad \text{at } x\leqslant x_T^- \quad (24a)$$

$$\Phi^*=\lambda\Phi \quad \text{at } x\geqslant x_T^+ \quad (24b)$$

$$\lambda=[\partial\Phi(x_T^-)/\partial x]/[\partial\Phi(x_T^+)/\partial x] \quad (24c)$$

$$\Phi=(\bar{\rho}\bar{C}-\rho_\ell C_L)/(\rho_\ell C_E)=[\beta\kappa+(1-\beta\kappa)\varepsilon]\phi-\phi_L \quad (24d)$$

where $x\leqslant x_T^-$ and $x\geqslant x_T^+$ represent, respectively, the mushy zone and the liquid region from the previous iteration. The use of λ is to achieve a continuous slope across the line of dendrite tips for the Φ^*-function. It can be verified that the value of Φ^* varies continuously from negative, zero to positive along a path from the mushy zone to the liquid region. Hence, the line of dendrite tips is well-defined by the curve of $\Phi^*=0$.

During the iterations, the value of ε is assigned zero and unity, respectively, for the solid and liquid region after the eutectic front and the line of dendrite tips are updated. It is interesting to note from equation (23) that the solute concentration in the interdendritic liquid of the mushy zone (ϕ) will approach $\phi_L(\theta)$ once the solution converges ($\tilde{\varepsilon}\approx\varepsilon$) within a prescribed tolerance, i.e.

$$\frac{\max|\psi-\tilde{\psi}|}{\psi_{\max}-\psi_{\min}}\leqslant Tol \quad (25)$$

where ψ and $\tilde{\psi}$ represent the solution $(\varepsilon,u,v,p,\theta,\phi)$ from the present iteration and that from the previous iteration, respectively.

PERFORMANCE OF THE LATENT HEAT METHOD

In this section, a one-dimensional solidification process of a binary alloy is illustrated in example 1 to examine the performance of the latent heat method, in case the natural convection is negligible. The effect of natural convection will be studied in example 2

through solidification of an NH_4Cl–H_2O solution inside a square enclosure.

Example 1—one-dimensional solidification of a binary alloy

Let the space between two parallel flat plates be fully filled with a quiescent liquid alloy. The liquid alloy is assumed to have a uniform initial solute concentration ϕ_0 and a uniform initial temperature $\theta_0 = 1$, such that the initial state of the liquid alloy is beyond its liquidus θ_L. At $\tau \geqslant 0$, the flat plate at $x = 0$ is cooled to a temperature ($\theta = 0$) below the eutectic temperature θ_E, while the other flat plate at $x = 1$ is maintained at $\theta = 1$. Natural convection is assumed negligibly small. Under this situation, the governing equations and the associated boundary conditions can be written as

$$\sigma\bar{\gamma}\frac{\partial\theta}{\partial\tau} + (1-\sigma)\frac{\partial f}{\partial\tau} = \frac{\partial}{\partial x}\left(k^*_{\text{eff}}\frac{\partial\theta}{\partial x}\right) \tag{26}$$

$$\sigma[\varepsilon + (1-\varepsilon)\beta\kappa]\frac{\partial\phi}{\partial\tau} + (1-\beta\kappa)\,\phi\frac{\partial\varepsilon}{\partial\tau} = \frac{\partial}{\partial x}\left(\varepsilon\, Le^{-1} D^*_{\text{eff}}\frac{\partial\phi}{\partial x}\right) \tag{27}$$

$$\theta(x,0) = 1 \quad \theta(0,\tau) = 0 \quad \theta(1,\tau) = 1 \tag{28}$$

$$\phi(x,0) = \phi_0, \quad \partial\phi(1,\tau)/\partial x = 0 \tag{29}$$

$$\phi(x_E,\tau) = 1 \text{ if } x_E \text{ exists, otherwise } \partial\phi(0,\tau)/\partial x = 0 \tag{30}$$

where $x = x_E$ is the location of the eutectic front. The parameters used for the computations were

$$\gamma = 1 \quad \beta = 1 \quad k_s/k_\ell = 1 \quad \kappa = 0.125$$
$$\theta_E = 0.45 \quad \theta_F = 1.45 \quad \theta_L = \theta_F - (\theta_F - \theta_E)\,\phi_L$$
$$Ste = 1 \quad \phi_0 = 0.5. \tag{31}$$

Numerical results were obtained for various Lewis numbers in the range of $2 \leqslant Le \leqslant 200$. The tolerance of convergence [equation (25)] was $Tol = 5 \times 10^{-5}$. The step size $(\Delta x, \Delta\tau) = (0.025, 0.01)$ was found adequate for all of the cases.

Figure 3 shows the variation of the eutectic front with time for the case of $Le = 2$. The lines of dendrite tips based on $\Phi^* = 0$ and $\varepsilon = 0.999$ are also plotted in Fig. 3 for comparison. The use of the artificial function Φ^* seems to successfully produce a smooth curve for the line of dendrite tips. Note that at the very beginning of the solidification process, the solute concentration near the dendrite tips is essentially at ϕ_0. Hence, the fast cooling at the boundary of $x = 0$ causes rapid growing rates for both solid region and mushy zone as observable from Fig. 3. In the late stage of the solidification process, however, the temperature gradient in the liquid region will increase due to the particular thermal boundary conditions, $\theta(x_E,\tau) = \theta_E$ and $\theta(1,\tau) = 1$. In addition, the rejected solute would accumulate in the interdendritic liquid such that the liquidus in the mushy zone will be significantly decreased. This might account for the fact that the solid region eventually stops growing at $\tau > 0.4$, while the mushy zone reaches its maximum thickness at $\tau = 0.08$ and completely remelts at $\tau > 0.33$.

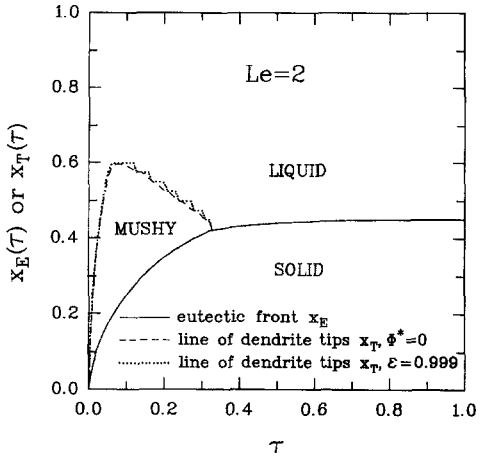

Fig. 3. Variations of the eutectic front and the line of dendrite tips with time for $Le = 2$ (example 1).

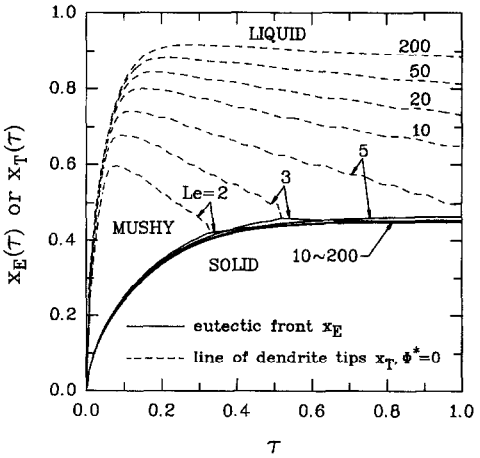

Fig. 4. Effect of Lewis number on the eutectic front and the line of dendrite tips (example 1).

Effect of the Lewis number on the eutectic front and the line of dendrite tips is shown in Fig. 4. For a large Lewis number (say $Le = 200$), the rejected solute in an early stage of the solidification process would pile up on the dendrite surface due to a poor solute diffusivity ($Le = \alpha/D \gg 1$). The dendrite thus holds rich solute when it grows further due to the strong cooling imposed at $x = 0$. This implies a lean solute for the liquid phase in late stage of solidification. Such a situation would give rise to a prosperous mushy zone (see Fig. 4), although the effect of the Lewis number on the eutectic front is negligibly small. The

mushy zone seems not to completely remelt when $Le \geqslant 5$.

Example 2—solidification of an NH_4Cl–H_2O *solution inside a square enclosure*

As mentioned earlier, Beckermann and Viskanta [6] performed an experiment to study the dendritic solidification of an NH_4Cl–H_2O solution. Their test cell has a square cross-section of $4.76 \times 4.76\ cm^2$. Both bottom and top walls of the test cell were well insulated, while the two vertical walls served as heat source/sink. The initial state of the NH_4Cl–H_2O solution was $(T_0, C_0) = (307.5\ K, 0.7)$ with C_0 denoting the mass fraction of water. At $t \geqslant 0$, one of the vertical walls was suddenly cooled and maintained at $T_\infty = 273.15$ K, which is above the eutectic temperature $T_E = 257.75$ K. The mushy zone thus started to form from the cold wall. No pure solid region was found inside the test cell. Such a solidification process can be simulated by the governing equations described in the previous section along with the boundary conditions

$$\begin{aligned}
&u = v = 0 \quad \theta = 1 \quad \phi = \phi_0 \quad \text{for } (x, y, 0)\\
&u = v = 0 \quad \theta = 1 \quad \frac{\partial \phi}{\partial x} = 0 \quad \text{for } (0, y, \tau)\\
&u = v = 0 \quad \theta = 0 \quad \frac{\partial \phi}{\partial x} = 0 \quad \text{for } (1, y, \tau)\\
&u = v = 0 \quad \frac{\partial \theta}{\partial y} = 0 \quad \frac{\partial \phi}{\partial y} = 0 \quad \text{for } (x, 0, \tau)\\
&u = v = 0 \quad \frac{\partial \theta}{\partial y} = 0 \quad \frac{\partial \phi}{\partial y} = 0 \quad \text{for } (x, 1, \tau) \qquad (32)
\end{aligned}$$

where $x = 1$ represents the cold wall. The corresponding parameters appearing in the governing equations are

$$\begin{aligned}
&Pr = 9.03 \qquad Ra = 8.639 \times 10^7 \qquad N = 12.58\\
&Ste = 0.3557 \qquad Le = 74.25 \qquad k_s/k_\ell = 0.84\\
&\gamma = 0.589 \qquad \theta_F = 10.459 \qquad \theta_E = -0.458\\
&\kappa(T) = 0.3 \qquad \phi_0 = C_0/C_E = 0.7/0.803 = 0.872\\
&\beta = 1.023 \quad \phi_L(\theta) = (\theta_F - \theta)/(\theta_F - \theta_E). \qquad (33)
\end{aligned}$$

In this example, computations were performed on a grid system of 101×101 nodal points with slightly clustered grids along the walls of the enclosure. The time step of $\Delta\tau = 1.548 \times 10^{-5}$ that is equivalent to $\Delta t = 1$ s in real time was used for the time coordinate. The convergence criterion $Tol = 5 \times 10^{-4}$ was employed.

Figure 5 shows the results of streamlines, isotherms and isopleths of solute concentration at $t = 3$ min. The line of dendrite tips is represented by the dashed curve. The discrepancy of the stream functions computed from the results of $u(x, y, \tau)$ and $v(x, y, \tau)$, i.e.

$$\psi(x, y, \tau) = \int_0^y u\,dy = -\int_0^x v\,dx \qquad (34)$$

is within 0.01%. Unlike previous studies, the present streamlines are quite smooth, even at the line of dendrite tips. Note also that, due to the presence of dendrite arms, the natural convection inside the mushy zone is very weak as compared to that in the pure liquid region. To properly present the flow field, streamlines with $\Delta\psi = 3$ is illustrated in Fig. 5(a) for the pure liquid region, while that with a small increment $\Delta\psi = 0.2$ is provided in Fig. 5(b) for the mushy zone. For a similar reason, isotherms with $\Delta\theta = 0.01$ and $\Delta\theta = 0.1$ and isopleths of concentration with $\Delta\phi = 0.0003$ and $\Delta\phi = 0.006$ are presented in Figs. 5(c)–(f), respectively. The results of streamlines, isotherms and isopleths of solute concentration for $t = 5$ min are shown in Fig. 6 with the same system of increments.

Figure 5 reveals a weak counter-clockwise circulation flow ($\psi_{max} = +2.4$) in the mushy zone and a strong clockwise circulation flow ($\psi_{min} = -50.48$) in the pure liquid region. This leads to a strong descending flow along the line of dendrite tips. As illustrated in Fig. 5(b), the interdendritic flow near the cold wall ($x = 1$) brings the rejected solute (water) to the top of the enclosure. Some of the solute then stays there to form a solute-rich top layer, while the remainder follows the descending flow to go down the bottom of the enclosure. Upon hitting the bottom, part of the solute-rich liquid turns into the clockwise circulation flow in the pure liquid region, while the other turns to right to complete the counter-clockwise circulation in the mushy zone. Hence, the space in between the two adjacent isopleths of $C = 0.7033$ and $C = 0.7093$ [see Fig. 5(f)] rapidly widens in a region near the enclosure bottom. These characteristics of the double-diffusive convection (including the formation of the solute-rich top layer) are more pronounced as time elapses, see Fig. 6 for instance.

Figure 7 shows the present prediction for the line of dendrite tips at $t = 3$ min. A tracing from a shadowgraph image of Beckermann and Viskanta's experiment [6] is also plotted in Fig. 7 for comparison. It is noted that the shadowgraph [6] also recorded the region of the solute-rich top layer, as indicated by marker A. Physically, the high solute concentration in the solute-rich top layer would depress the growth of the mushy zone such that the mushy zone should have a small thickness on the top of the enclosure. The present result seems to correctly reflect this point. In their experiment, Bekermann and Viskanta [6] found that some of the dendrites were not firmly attached to the cold wall ($x = 1$). These loose dendrites followed the above-mentioned descending flow and deposited on the bottom of the liquid region (see Fig. 7). Although such an effect is not considered in the present study, the present prediction on the total volume of mushy zone has a good agreement with the experimental result, as observable from Fig. 7.

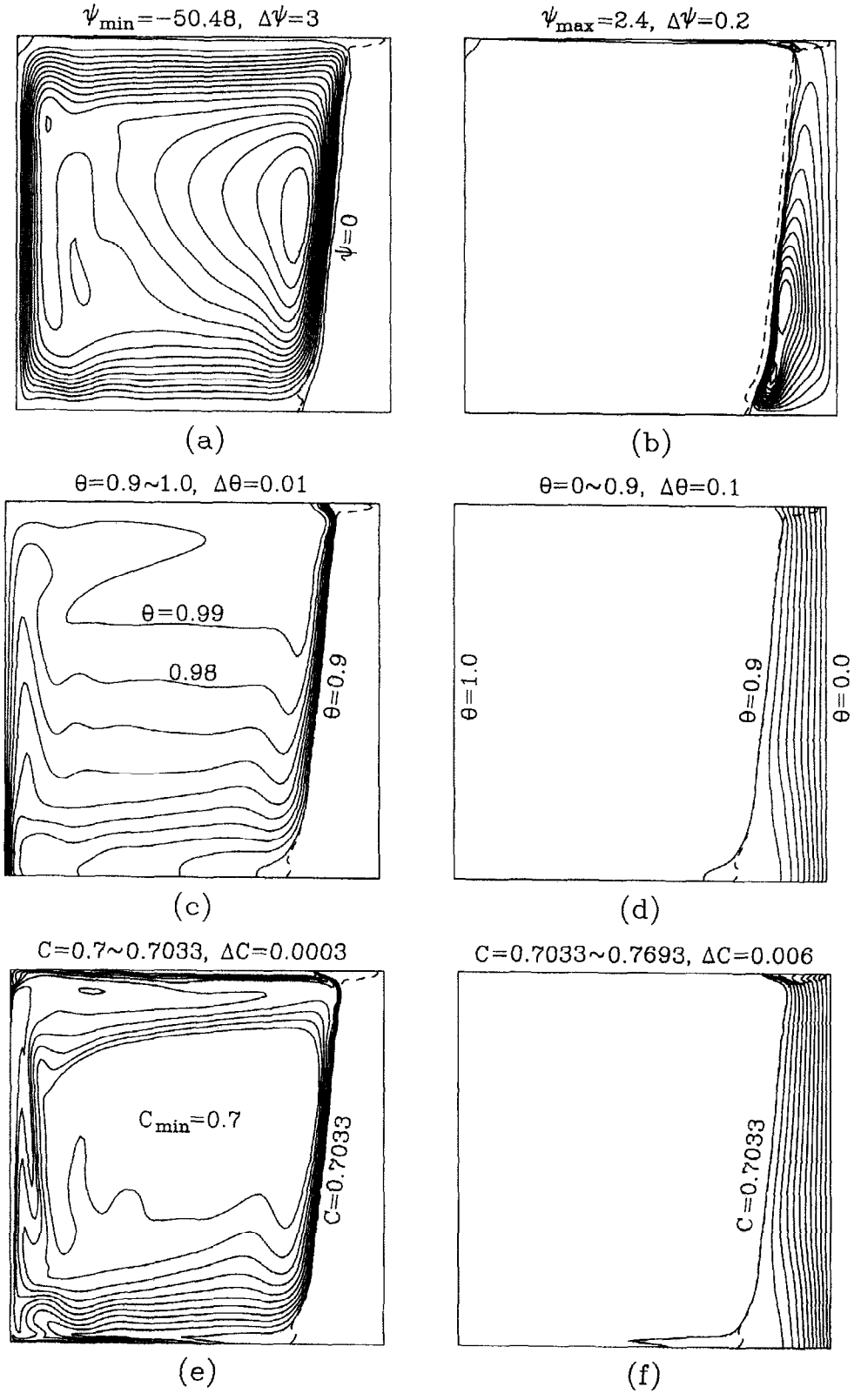

Fig. 5. Present prediction of streamlines, isotherms and isopleths of solute concentration for example 2 at $t = 3$ min.

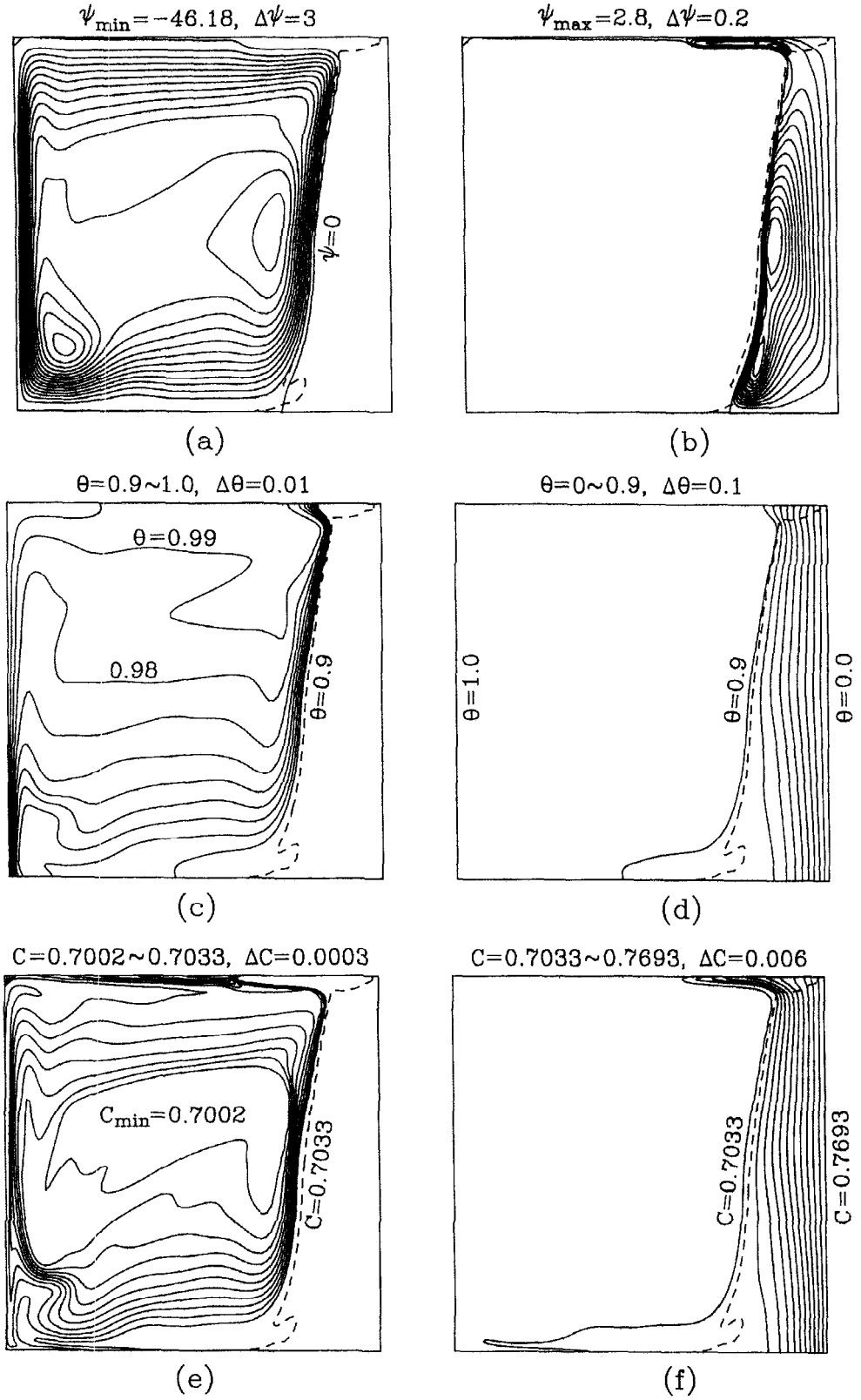

Fig. 6. Present prediction of streamlines, isotherms and isopleths of solute concentration for example 2 at $t = 5$ min.

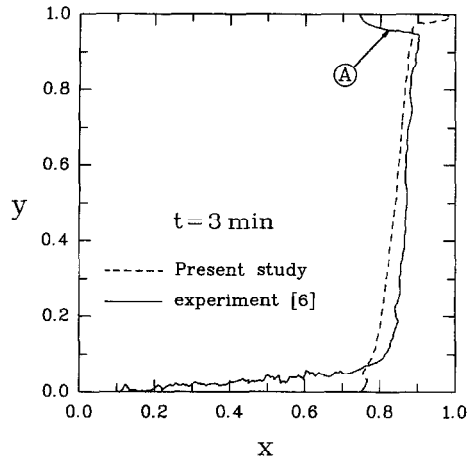

Fig. 7. Comparison of the line of dendrite tips for example 2 at $t = 3$ min.

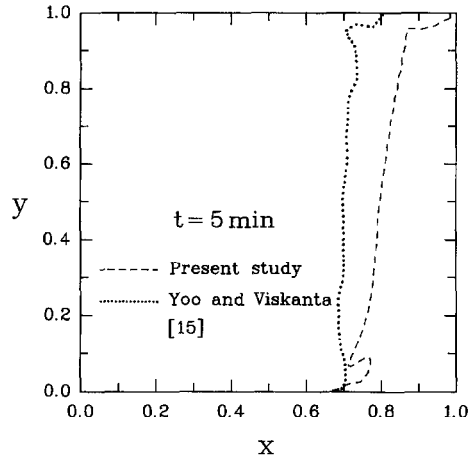

Fig. 8. Comparison of the line of dendrite tips for example 2 at $t = 5$ min.

Figure 8 shows a comparison of the present prediction with that of Yoo and Viskanta [15] on the profile of the line of dendrite tips at $t = 5$ min. On Fig. 8 a large discrepancy between the two predictions is observed. For instance, the present result of mushy zone thickness at $y = 0.5$ (or $Y = 2.38$ cm) is 0.98 cm as compared to 1.43 cm predicted by Yoo and Viskanta [15]. This discrepancy is obviously not due to the effect of anisotropic permeability in the mushy zone [15]. Unfortunately, there are no shadowgraphs available for the particular time of $t = 5$ min. In their study, Yoo and Viskanta [15] predicted that the thickness of the mushy zone at $y = 0.5$ increased from 2.10 to 2.20 cm as time elapsed from 15 to 20 min. Its counterpart in the experiment [6], however, grew only from 1.12 to 1.28 cm. Their numerical procedure seems to overpredict the mushy zone thickness by 80%. Hence, the thickness of the mushy zone in the experiment [6] can be roughly estimated by $1.43/1.8 \approx 0.79$ cm for $(y, t) = (0.5, 5$ min). This estimation is close to $0.98 \times 0.8 \approx 0.78$ cm, if one assumes that the mushy zone thickness (at $y = 0.5$) in the experiment is 80% as large as that predicted by the present method (see Fig. 7). Therefore, the present prediction is believed to agree with the experimental result as well for $t = 5$ min, if the effect of the descending detached-dendrite can be properly considered in the computations.

CONCLUSION

In solidification process of a binary alloy, there could be a two-phase region known as mushy zone between the solid region and the liquid region. The mushy zone and the solid region are separated by the eutectic front. Physically, a great amount of latent heat could be suddenly released from an area when the eutectic front sweeps through that area. In addition, both the pressure-linked equation and the species equation become trivial in the solid region. In the present study, a modified latent heat method is employed to handle the abruptly released latent heat from the eutectic front.

The eutectic state (C_E, T_E) and the no-slip condition are imposed on the eutectic front such that there is no need to solve the momentum and species equation in the solid region. Fortunately, the weighting function scheme along with the NAPPLE algorithm is found to solve the transport equations quite efficiently in such an irregular domain consisting of the mushy zone and liquid region. As illustrated in example 1, the present method successfully predicts the physical phenomenon that the rejected solute accumulated in front of dendrite tips could cause remelt of dendrites. From a simulation of solidification process in an NH_4Cl–H_2O solution (example 2), the present method was found capable of resolving the double-diffusive phenomena observed in the experiment. Furthermore, the total volume of mushy zone predicted by the present method shows a satisfactory agreement with the shadowgraphs of the experiment.

Acknowledgement—The authors wish to express their appreciation to the National Science Council of the Republic of China in Taiwan for the financial support of this work through the project NSC83-0401-E007-042.

REFERENCES

1. W. D. Bennon and F. P. Incropera, A continuum model for momentum, heat and species transport in binary solid–liquid phase change systems—I. Model formulation, *Int. J. Heat Mass Transfer* **30**, 2161–2170 (1987).
2. W. D. Bennon and F. P. Incropera, A continuum model for momentum, heat and species transport in binary solid–liquid phase change systems—II. Application to solidification in a rectangular cavity, *Int. J. Heat Mass Transfer* **30**, 2171–2187 (1987).
3. P. J. Prescott and F. P. Incropera, Modeling of dendritic solidification systems: reassessment of the continuum equation, *Int. J. Heat Mass Transfer* **34**, 2351–2359 (1991).
4. V. R. Voller, A. D. Brent and C. Prakash, The modelling of heat, mass and solute transport in solidification

systems, *Int. J. Heat Mass Transfer* **32,** 1719–1731 (1989).
5. M. Rappaz and V. Voller, Modeling of micro-macrosegregation in solidification process, *Metall. Trans.* **21A,** 749–753 (1990).
6. C. Beckermann and R. Viskanta, Double-diffusion convection during dendritic solidification of a binary mixture, *Physicochem. Hydrodyn.* **10,** 195–213 (1988).
7. S. Ganesan and D. R. Poirier, Conservation of mass and momentum for the flow of interdendritic liquid during solidification, *Metall. Trans.* **21B,** 173–181 (1990).
8. J. Ni and C. Beckermann, A volume-averaged two-phase model for transport phenomena during solidification, *Metall. Trans.* **22B,** 349–361 (1991).
9. M. Rappaz, Modelling of microstructure formation in solidification processes, *Int. Mater. Rev.* **34,** 93–123 (1989).
10. R. Viskanta, Mathematical modeling of transport processes during solidification of binary systems, *JSME Int. J.* **33,** 409–423 (1990).
11. M. C. Flemings, *Solidification Processing*. McGraw-Hill, New York (1974).
12. S. L. Lee and R. Y. Tzong, An enthalpy formulation for phase change problems with a large thermal diffusivity jump across the interface, *Int. J. Heat Mass Transfer* **34,** 1491–1502 (1991).
13. R. Y. Tzong and S. L. Lee, Solidification of arbitrarily shaped casting in mold-casting system, *Int. J. Heat Mass Transfer* **35,** 2795–2803 (1992).
14. W. Kurz and D. J. Fisher, *Fundamentals of Solidification* (3rd Edn). Trans. Tech. Publications, Aedermannsdorf (1989).
15. H. Yoo and R. Viskanta, Effect of anisotropic permeability on the transport process during solidification of a binary mixture, *Int. J. Heat Mass Transfer* **35,** 2335–2346 (1992).
16. S. L. Lee and R. Y. Tzong, Artificial pressure for pressure-linked equation, *Int. J. Heat Mass Transfer* **35,** 2705–2716 (1992).